# Chapter 4

# Temporal Self-Organization in Formic Acid Oxidation - Experimental

## 4.1 Introduction

> "*Wenn es als nachgewiesen betrachtet werden kann, daß die Umkehrungen, von denen die Rede gewesen ist, wirklich von einer Veränderung der Metalloberfläche abhängen, so müßte es nun von Wichtigkeit seyn, die Beschaffenheit dieser Umstände auch chemisch nachzuweisen. Ich gestehe aufrichtig, daß ich für die Fälle, wo es gerade am wichtigsten wäre, hierüber Aufschluß zu erhalten, keinen Weg dazu weiß.*"
>
> M.G.Th. Fechner, Jahrbuch der Chemie und Physik, **53**II (**1828**) 147

Over the last few decades, impressive technological strides forward have been made in order to investigate the real state of the electrochemical interface during oscillatory processes. Alongside with an increasing number of sophisticated, experimental studies, a growing number of theoretical speculations as to the detailed mechanistic origin of the oscillatory instabilities in certain systems have also been put forward.

The first observation of temporally periodic instabilities during the electrocatalytic oxidation of formic acid (FA), HCOOH, dates back almost seventy years [110, 111]. This early work was performed on electrodes of Rh , Pt and Pd under galvanostatic control [111, 112, 113, 114, 115, 116, 117, 118, 119, 120]. In the case of Pt, focus was first placed on polycrystalline studies [121, 122, 123, 124, 125]. Finally, an important step towards an understanding of the relevant chemical processes was achieved when, from the early eighties on, single crystals, predominantly Pt, were introduced as working electrodes [126, 127, 128, 90, 129, 130, 88, 131, 132, 133, 134, 135]. Sophisticated experimental techniques were employed to investigate the system's mechanism such as IR spectroscopy [136, 20, 137, 116], mass spectroscopy [138, 139, 140, 141], EQMB (Electrochemical quartz microbalance) [142] as well as ex-situ methods under

Ultra-High-Vacuum [143, 144]. These studies of the pure formic acid oxidation system were complemented by the investigation of the effect of coadsorbed metals such as Bi [145, 146], Sb [147]or Bi and As [148, 149]. All these experimental studies provided a clear idea as to which chemical processes and which intermediates are involved in the oxidation process. In particular, the nature of the poisoning intermediate which has long been the subject of hot controversaries [138, 150, 137] could be resolved. Vibrational data [151, 116, 137] clearly indicated that linear, bridged and trifold $CO$ - depending on the potential and the coverage- is the major surface poison which is oxidized to the final product $CO_2$ at higher potentials.

There are only few studies dealing with oscillations of the measured current during FA oxidation on low-index Pt single crystals [130, 88, 131, 132] under potentiostatic control. These studies provide similar physicochemical interpretations of the current oscillations assuming formic acid to be oxidized via a direct and an indirect reaction path (*dual-path mechanism* [122, 152]). The periodic adsorption and reactive removal of CO by adsorbed oxygen species (possibly combined with periodic changes in the surface structure [131] or the local pH [130, 88, 132]) is identified with the experimental current oscillations. In ref. [131, 132], the authors proposed an autocatalytic removal of CO in order to account for the observed instabilities, whereas ref. [130, 88] found the FA oxidation mechanism to contain unstable network features. Thus, all potentiostatic FA studies emphasized purely chemical sources of instability, whereas the role of the ohmic resistance $R$ was not explicitly considered.

The potentiostatic studies are in agreement as to the significant difference between the single crystal planes, but differ considerably in the results concerning the role of mass transport and the local pH. Pt(100) was found to reproducibly show current oscillations, whereas on Pt(110) and Pt(111) oscillatory behavior was also reproducible but more strongly dependent on pretreatment.

In this chapter, a detailed experimental analysis of current oscillations during FA oxidation occuring on the three low-index Pt planes will be presented [153]. The study will be preceeded by an investigation of the current/potential behavior of the electrochemical $CO$ oxidation (section 3) which can be considered as a subsystem of the FA system. Section 4 first considers the current/potential characteristics during formic acid oxidation on Pt(100), Pt(110) and Pt(111) at low ohmic resistance before addressing the complex oscillatory instabilities seen in the cyclovoltammograms (CVs) at higher ohmic resistances. Furthermore, we focus on current oscillations and, finally, report the observed effects when stirring is applied.

## 4.2 Experimental

All potentials given in this chapter refer to the standard calomel electrode (SCE). In the main compartment low-index Pt single crystals Pt(100), Pt(110) and Pt(111) ( $\approx$ 0.6 $cm^2$ each) were used as working electrodes. In order to avoid crystal edge effects, the working electrode was first dipped into the electrolyte and then pulled out as far as possible such that the electrolyte was exclusively in contact with the oriented surface [154].

The pretreatment of the single crystals was as follows: First, they were annealed

at 1500 K in a Bunsen flame for about 1 min. The crystals were then cooled in an $N_2$ atmosphere for at least 5 min and rapidly transferred into the electrochemical cell [155]. Flame annealing became necessary whenever the applied sweep potentials reached values where surface roughening sets in.

All electrolyte solutions (1 M $Na_2SO_4$ saturated with gaseous CO for the CO oxidation experiments and 0.05 M HCOOH in $10^{-3}$ M $HClO_4$ and 1 M HCOONa in 0.5 M $H_2SO_4$ for experiments involving formic acid) were prepared with tridestilled water. $H_2SO_4$ and $HClO_4$ (Merck) were purchased as suprapure chemicals and were used without further purification. HCOOH, HCOONa, $Na_2SO_4$,$NaClO_4$ and NaOH were employed with p.A. purity. Before each measurement of section 3, first an $N_2$ (5N) gas stream was bubbled through the solution in order to remove dissolved oxygen. Thereafter, CO (4.7 N) gas was extensively bubbled through the electrochemical cell to achieve saturation. The gas stream was maintained during CO oxidation experiments ensuring a CO atmosphere. The degree of saturation was monitored by means of the measured current densities. In order to match the pH conditions of the formic acid experiments, the CO saturated solution was set to pH$\approx$ 2.7 using sulphuric acid. Before and during the experiments on formic acid, a $N_2$ gas stream was bubbled through the cell electrolyte in order to keep the cell free of air.

Stirring was achieved by means of a magnetic stirrer sitting on the bottom of the cell. The measurements were performed at room temperature throughout.

## 4.3 Electrochemical CO-Oxidation

There is significant evidence that the electrochemical formic acid oxidation partially proceeds via a surface poison which is oxidized by oxygen-containing species forming at higher double-layer potentials. The poisonous intermediate was recently identified to be CO [20, 137, 116, 151]. Consequently, the electrochemical CO-oxidation system can be thought of as a simple submechanism of that of formic acid oxidation. In the following we report experiments on CO-Oxidation in solution of high ionic conductivity (1 M $Na_2SO_4$) in order to avoid any electrochemical instabilities.

Fig. 4-1 shows the scanned $I/U$ curves of the three low-index Pt single crystals Pt(100), Pt(110) and Pt(111) for two different upper limit potentials. All three surfaces are seen to exhibit two different states for small and high values of the outer potential $U$, respectively: At low potentials of $U$, the surface is poisoned by CO and the current density vanishes, whereas at higher values of $U$ oxygen-containing species deactivate the surface. The blockage of the surface by oxygen species, however, is not complete in the potential range considered, since a current is observed in the high-potential state suggesting an ongoing diffusion-limited oxidation of CO despite of oxygen inhibition. Between the two constant current plateaus a sharp CO-oxidation peak is visible on the anodic scan, whereas a smoother transition occurs sweeping cathodically towards the CO covered state. One immediately recognizes that the potential range over which the CO poisoning occurs on the cathodic scan is shifted towards smaller values of $U$ compared to the potential range of CO removal during the anodic scan. This effect remains even for turning potentials right past the CO-oxidation peak indicating that it is not entirely due to irreversible oxide forma-

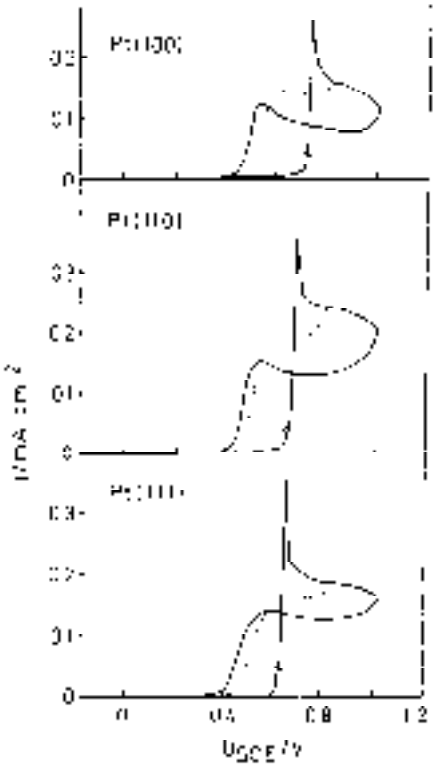

Figure 4-1: Experimental cyclovoltammograms (CVs) of the CO oxidation at Pt(100), Pt(110) and Pt(111) single crystal surfaces. Electrolyte: 1M $Na_2SO_4$, pH 2.7, saturated with CO. scan rate 10 mV/s, magnetic stirring.

tions. At first sight, this behavior suggests the coexistence of two values of $I$ for one given value of $U$. In order to doublecheck for such a coexistence, the CO-oxidation system was subject to galvanostatic conditions: As the current was increased in small increments from zero up to the diffusion limiting current of Fig. 4-1, no value of $I$ could be found for which $U$ decreased with increasing $I$ (negative $I/U$ characteristic). Such a characteristic corresponding to the potentiostatically unaccessible, unstable steady-state branch is expected in the presence of a true potentiostatic bistability. Instead, there was a identical, reversible one-to-one correspondence between current values $I$ and the outer potentials $U$ on both scan directions.

The stationary measurements reveal that the $I/U$ behavior of CO removal coincides under scanned and stationary conditions, whereas the CO poisoning is shifted to higher values of $U$ in the stationary case.

Fig. 4-1 further reveals that the CO oxidation peak does not coincide for the three single crystals. Instead, the current $I$ rises at increasingly smaller values of $U$ on the anodic sweep going from Pt(100) to Pt(110) and to Pt(111).

For the sake of comparison, Fig. 4-2 shows a typical $I/U$ behavior of the CO

system on a rotating polycrystalline Pt electrode. Here, the mass transport is much better defined compared to magnetic stirring. The values of current densities are higher; however, the overall behavior of the electrochemical system is seen to be qualitatively unchanged.

Figure 4-2: Experimental CVs of the CO oxidation (a) and the OH adsorption and desorption (b) on a rotating disk electrode (Pt poly) with stirring of 3000 rpm, scan rate 20 mV/s. Electrolyte: 1 M $Na_2SO_4$, pH 2.7; saturated with CO (a), saturated with $N_2$ (b)

## 4.4 Electrochemical HCOOH Oxidation

We report cyclovoltammetric measurements on Pt(100), Pt(110) and Pt(111). The cyclovoltammograms are complemented by measurements of the temporal evolution of the current $I$ for a constant potential $U$. Except for the upcoming section on stirring effects, all CVs and current oscillations were measured without stirring the electrolyte.

### 4.4.1 $I/U$ characteristics at low ohmic resistances

Fig. 4-3 shows the CVs of the three single crystal surfaces at a scan rate of 10 mV/s in a solution of high ion conductivity, i.e. almost vanishing ohmic resistance $R$.

One recognizes the typical current-potential characteristics of self-poisoning oxidation reactions of small organic compounds [88, 135, 132, 20]. Starting at low values of the outer potential $U$, Pt(100) and Pt(110) show a very similar behavior: a high degree of poisoning of the surface in the potential region 0.2-0.5 V results in a low current density. The small peak observed in this region will be referred to as peak I [122, 156]. At higher values of $U$ (0.55-0.6 V), adsorption with oxygen species (OH) starts leading to an activation of the surface by oxidation of the poisoning species. The current increases considerably. In the following, this current peak will be referred

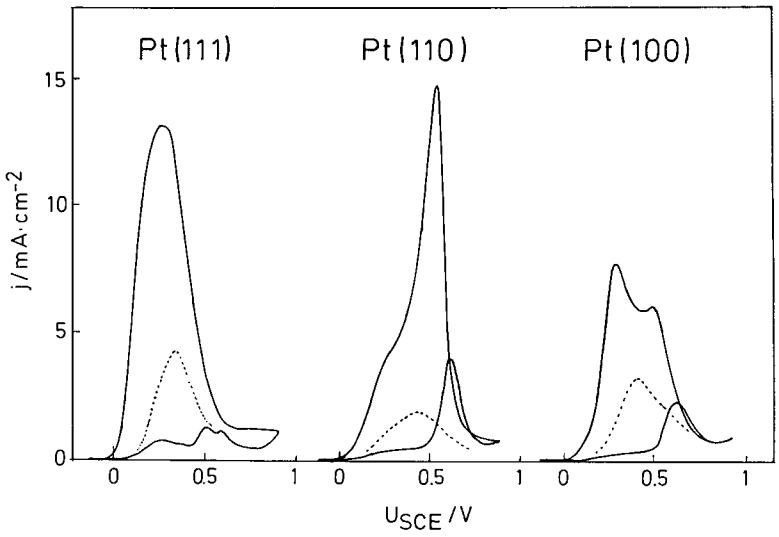


Figure 4-3: $I/U$ characteristics for the oxidation of formic acid (FA) on the three Pt single crystal surfaces. Electrolyte: 1M HCOONa + 0.5M $H_2SO_4$, pH 2.6 , without stirring. Solid curve: scanned with 10 mV/s, dashed curve: stationary behavior

to as peak II [156]. Further increase of $U$ up to 0.8-0.9 V leads back to a deactivated surface due to the coverage of oxygen species. Note that the current density does not decrease back to the values where it started when the surface was poisoned. Instead, the current stays at around 1 mA/cm$^2$ indicating an incomplete inhibition of formic acid oxidation by the OH coverage. At considerably higher values of $U$, a third anodic peak (peak III) occurs [121, 122] which, however, will not be considered in this study since the potential sweep was reversed as soon as the surface had been deactivated past peak II.

On the reversed scan of Pt(100) and Pt(110), the surface gets reactivated very rapidly as soon as the OH species desorb (0.6-0.5 V). Now, the surface is almost free of poisoning species and the oxidation of formic acid proceeds in an unhindered manner which leads to a large current peak referred to as peak IV. Scanning to more negative potential, however, the CV reveals another current peak around 0.25 V for both Pt(100) and Pt(110) (referred to as peak V). Whereas on Pt(100) peak IV is smaller than peak V, the reverse holds for Pt(110), where peak V appears as a shoulder of peak IV.

In contrast to Pt(100) and Pt(110), Pt(111) shows a distinct peak I and a small splitted peak II. Furthermore, on the cathodic scan there is no separation between peak IV and V. Instead, both peaks merge into one broad current peak.

Further investigation of the characteristics of peak IV and V revealed a complex dependence of both peaks on the scan rate and the anodic limit potential: Fig. 4-4a and b show the dependence of peak IV and peak V on the upper limit potenial. The

negative portion of the $I/U$ curve of the pure electrolyte without formic acid is shown in Fig. 4-4c to compare the potential regions of peak IV and V and the potential at which the deposited (ir)reversible surface oxides are reduced. The experiments suggest a strong increase of peak IV with the upper turning potential (going from dotted, dashed to solid) on both surfaces (on Pt(110) even more drastic than on Pt(100)). The effect of the turning potential on peak V, however, differs significantly on Pt(100) and Pt(110): Whereas an increase in turning potential leads to a small increase of the shoulder-like peak V on Pt(110), it results into a moderate decrease of peak V on Pt(100). Subfigure c again confirms that peak IV occurs at values of $U$ where the rate of desorption/reduction of OH reaches its maximum.

On Pt(100) as well as on Pt(110), peak IV was found to increase at higher sweep rates. peak V, however, remained unchanged on Pt(110), but increased on Pt(100).

Looking at the CVs of Fig. 4-4 and 4-3 one might be tempted to infer from the different current densities during the anodic and cathodic scan the presence of a bistability somewhere in the considered potential interval. The stationary $I/U$-curves, however, (dotted line in Fig. 4-3) reveals the kinetic nature of the differences in current densities. If one stops the potential sweep on peak IV, for instance, the current eventually decreases down to the dotted line. For each value of $U$ there exists exactly one value of $I$. Thus, in agreement to what has been pointed out in the introduction there is no electrochemical instability present in the system for a small value of $R$.

### 4.4.2 Instabilities at high values of $R$

In the introduction, a general argument has been given in order to explain the instability occurring at sufficiently high values of $R$. Fig. 4-5 illustrates this idea schematically for the CV of Pt(100) given in Fig. 4-3c and provides a qualitative explanation of the observed shapes of the CV. In Fig. 4-5a, the CV of Pt(100) is shown without an additional external series resistance $R_{ex}$. Increasing $R_{ex}$ and correcting the CV by the value of the $IR$ drop results in the distortion of the original CV as can be seen by the dotted line in Fig. 4-5b and 4-5c. Note that the dotted $I-U$ curve is not entirely accessible, i.e. does not correspond to a real CV. Instead, the solid line in Fig. 4-5b and 4-5c schematically sketches out the CV that one would measure during a cathodic and anodic potential scan if no oscillatory instabilities were present. Scanning anodically, one can see that peak II becomes strongly asymmetric; at the turning point the current falls off abruptly to low values. On the reversed scan in Fig. 4-5c, the current remains low even beyond the potential at which the current fell off from peak II. At even lower potential the current increases again abruptly and follows the dotted curve down to low values of $U$. Thus, bistability is generated with a sufficiently large external resistance.

Fig. 4-6 shows the measured $I-U$ curves for the three single crystal surfaces at a concentration of 0.05 M HCOOH in $10^{-3}$ M $HClO_4$. In accordance to the previous paragraph, all CVs are distorted towards slightly higher values of $U$ as compared to the curves of Fig. 4-3. For Pt(100) high current spikes occur on the cathodic scan, whereas Pt(110) exhibits high frequency spikes on peak II. Pt(111), in contrast, does

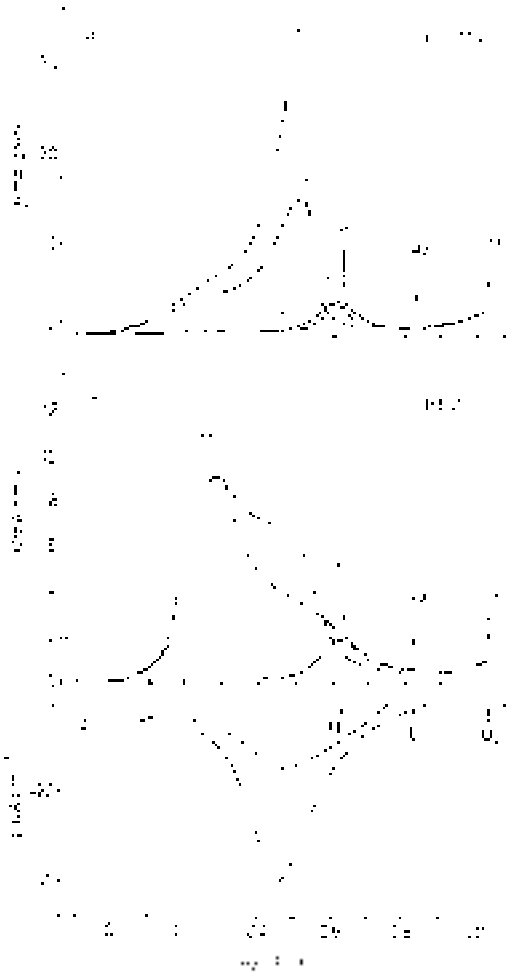

Figure 4-4: $I/U$ curves of the FA oxidation (a) and (b), and OH desorption (c) at Pt(110) and Pt(100). Electrolyte: 1M HCOONa + 0.5 M $H_2SO_4$, pH 2.6 (a) and (b), 1M $Na_2SO_4$, pH 2.6. The scan (20 mV/s) was reversed at different anodic potentials as indicated by the arrows.

not show any spiking.

In order to determine whether the ohmic resistance of the electrolyte is crucial for the observed instabilities, the $I-U$ characteristics of Pt(100) (Fig. 4-6c) were monitored for decreasing values of $R$. The decrease of $R$ was achieved by the successive addition of $NaClO_4$. In Fig. 4-7a, one clearly sees how the current spikes disappear as the ohmic resistance is decreased. After the addition of $1.6 \times 10^{-1}$ M $NaClO_4$ the CV of Pt(100) equals the one shown in Fig. 4-3c. Conversely, in Fig. 4-7b it is shown that starting with a CV of Pt(100) similar to that given in Fig. 4-3c and increasing the ohmic resistance $R$ by adding an external resistor $R_{ex}$ one induces the current

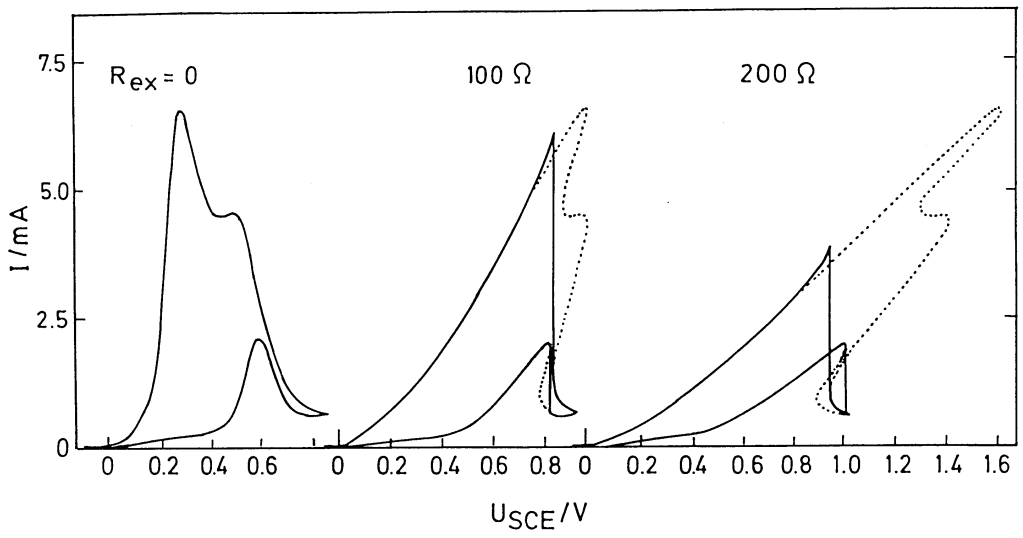


Figure 4-5: Effect of an increasing external ohmic resistance $R_{ex}$ on an experimental CV of the FA oxidation reaction measured in solution of high ionic conductivity and with $R_{ex} = 0, U \approx \phi$. Subfigure (a) shows the experimental CV on Pt(100) in 1 M HCOONa, 0.5 M $H_2SO_4$, scan rate 10 mV/s (see Fig. 3). Subfigure (b) and (c) display the calculated $I/U$ curves according to $U = \phi + IR$ for $R_{ex} = 100\Omega$ and $R_{ex} = 200\Omega$, respectively as dashed curves. The experimental CVs expected in the presence of an external ohmic resistance (cases (b) and (c)) are shown by the solid curves. It is seen that some parts of the dashed curve are not accessible experimentally. Furthermore, the generation of a hysteresis (bistability) is observed in the solid scanned curves at a sufficiently high value of $R_{ex}$.

spikes which indicate instability. It can be concluded that the observed instabilities require a sufficiently large ohmic resistance $R$.

### 4.4.3 Current oscillations at fixed values of $U$

#### Low HCOOH concentration

Unless stated otherwise, the bulk electrolyte used in the following contained 0.05 M HCOOH and $10^{-3}$ M $HClO_4$. During most measurements an additional external resistor $R_{ex}$ was used in series to the electrochemical cell.

**Pt(100)**. Fig. 4-8a depicts the measured CV with $R_{ex} = 600\Omega$. On the cathodic scan there are the current spikes as in Fig. 4-6, but now there are also current spikes visible on peak II indicating a regime of current oscillations. A small region of bistability is discernible between the potential of reactivation on the cathodic scan and the potential of oxygen blocking past peak II. To check a possible correspondence of the oscillatory potential range of both scan directions, the anodic scan was stopped

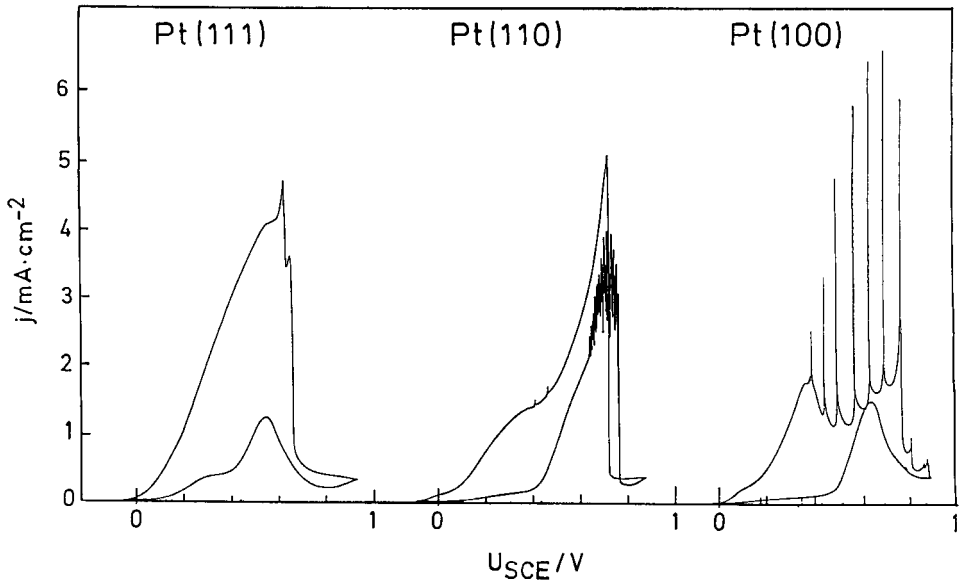


Figure 4-6: CVs of FA oxidation on the three Pt single crystal surfaces at low concentrations of FA and of the bulk electrolyte: 0.05 M HCOOH, $10^{-3}$ M $HClO_4$, scan rate 10 mV/s.

at different potentials on the ascending flank of peak II. In fact, stable relaxational current oscillations were finally obtained where a smooth curve has been obtained when scanning. Fig. 4-8b directly contrasts the waveforms of the current oscillations obtained when holding the potential in the anodic and the cathodic scan. The qualitative agreement of the oscillatory waveforms is clearly seen. The oscillations are characterized by a gradual increase of the current density followed by a very rapid decrease due to the poisoning reaction. Furthermore, the oscillations at higher values of $U$ are more relaxational and of larger amplitude than those at lower values of $U$ indicating a Hopf bifurcation at low values of $U$.

**Pt(110)**. In Fig. 4-9a a CV of the (110) surface is given with $R_{ex} = 80\,\Omega$. The anodic scan is drawn as solid line, whereas for the sake of clarity the reversed is shown as dashed line. Similar to Fig. 4-6b, there is a potential region on peak II where high-frequency current spikes occur. No current spikes are seen on the cathodic scan. Fixing the potential inside the current spike region, leads to transient current oscillations as given in Fig. 9b for $U = 704\,mV$ and $U = 725\,mV$. The life time of the oscillations is about one minute. Thereafter, the current remains low due to high OH coverage. Looking at the waveform of the oscillations, one recognizes a delayed current decrease, i.e. a slower poisoning process as compared to Pt(100), but a very rapid increase in current density.

**Pt(111)**. In contrast to the CV given in Fig. 4-6a, the CV shown in Fig. 4-10a was recorded with $R_{ex} = 430\Omega$. Several broad current spikes can be seen on the

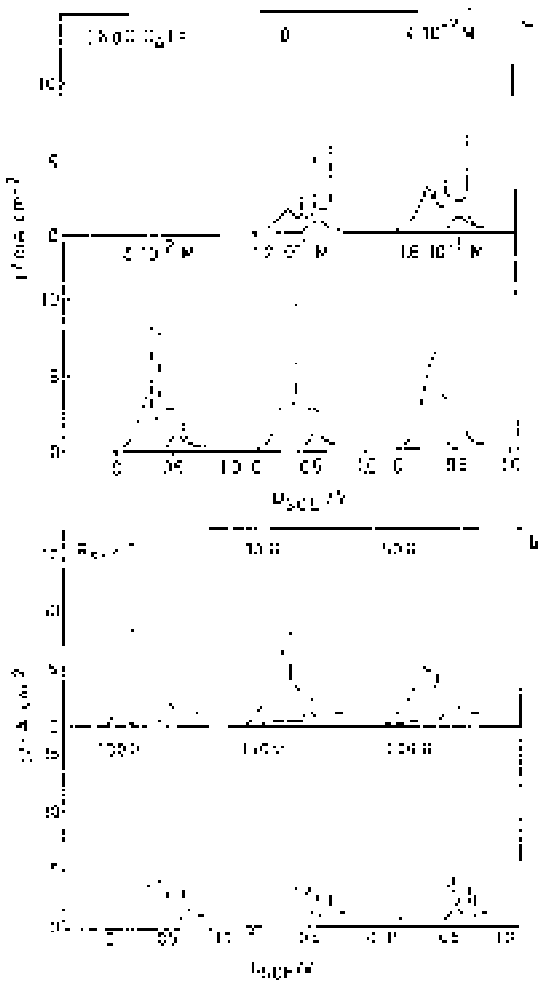

Figure 4-7: a) CVs of FA oxidation on Pt(100) for increasing ionic conductivity of the bulk electrolyte in the absence of any external resistance. Initial bulk solution: 0.05 M HCOOH, $10^{-3}$ M $HClO_4$. Increase in conductivity is achieved by addition of different amounts of $NaClO_4$. Scan rate 10mV/s throughout. b) CVs of FA oxidation on Pt(100) for increasing external ohmic resistances. bulk solution: 1 M HCOONa, 1 M HCOOH, pH 3.0. Scan rate 10 mV/s throughout.

ascending flank of peak II. No spikes could be observed on the cathodic scan. Here, the hysteresis of the transition between a predominantly CO-covered surface and a predominantly oxygen covered surface is very pronounced. Stopping the anodic scan at 965 mV, transient current oscillations evolved eventually falling off peak II as shown in Fig. 4-10b. Note the extremely long poisoning process leading to a slow decrease of the current density followed by the very rapid increase in the current due to the

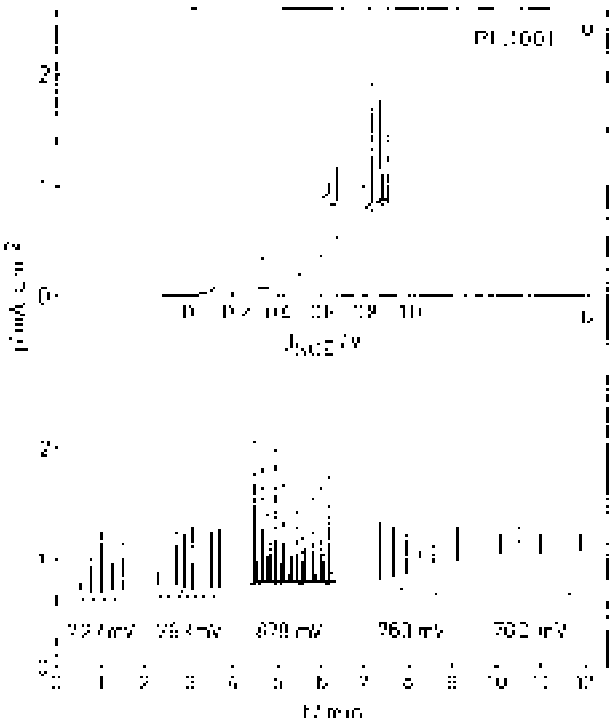

Figure 4-8: a) CV of FA oxidation on Pt(100) with external resistance $R_{ex} = 600\Omega$ at low FA concentration. Bulk solution: 0.05 M HCOOH, $10^{-3}$ M $HClO_4$. Scan rate 5 mV/s. Sharp current spikes appear on both the anodic and the cathodic scan indicating oscillatory behavior of the current.b) Current oscillations after holding the scan at different potentials $U$. From left to right, the first three times series were obtained when stopping on the anodic scan, the remaining two ones when stopping on the cathodic scan.

removal of the poison. In Fig. 4-10a, near the edge of peak II, where the $I-U$ curve abruptly falls off, some high-frequency small-amplitude spikes are also discernible in the observed CV. Similar spiking is observed during the time series of Fig. 4-10b. For longer observation times, however, this phenomenon seems to disappear as seen for the second portion of the time series in Fig. 4-10b. It should be added that , especially for low HCOOH concentrations, oscillations on Pt(111) are comparatively difficult to obtain as has been stated by various authors [88, 131].

### High HCOOH concentration

In addition to the current oscillations found on the low-index single crystal surfaces at low concentration, dynamical instabilities were also observed for considerably higher bulk concentration of HCOOH. The following experiments were performed in a sup-

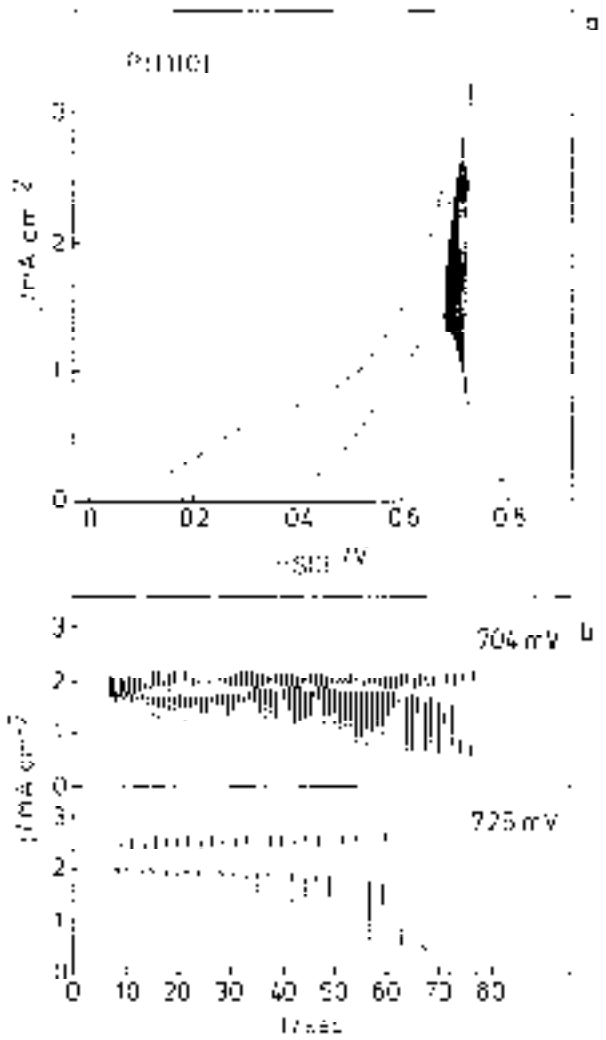


Figure 4-9: a) CV of FA oxidation on Pt(110) with external resistance $R_{ex} = 80\Omega$ at low FA concentration. Bulk solution: 0.05 M HCOOH, $10^{-3}$ M $HClO_4$. Scan rate 5 mV/s. Sharp current spikes appear on the anodic scan only.b) Current oscillations when the scan was stopped at 704 mV and 725 mV.

porting electrolyte containing 1 M HCOONa and 0.5 M $H_2SO_4$.

**Pt(100)**. For $R_{ex} = 390\,\Omega$ the (100) surface exhibits a rich variety of oscillatory states. Fig. 4-11 displays the measured CV at 5 mV/s. Unlike the CV at low concentration, there is a broad potential region of visible large-amplitude current spikes on the cathodic flank of peak II. Looking at this region more closely further reveals that small high-frequency spikes appear between the large spikes which suggests the presence of mixed-mode oscillations. Stationary measurements of the current at dif-

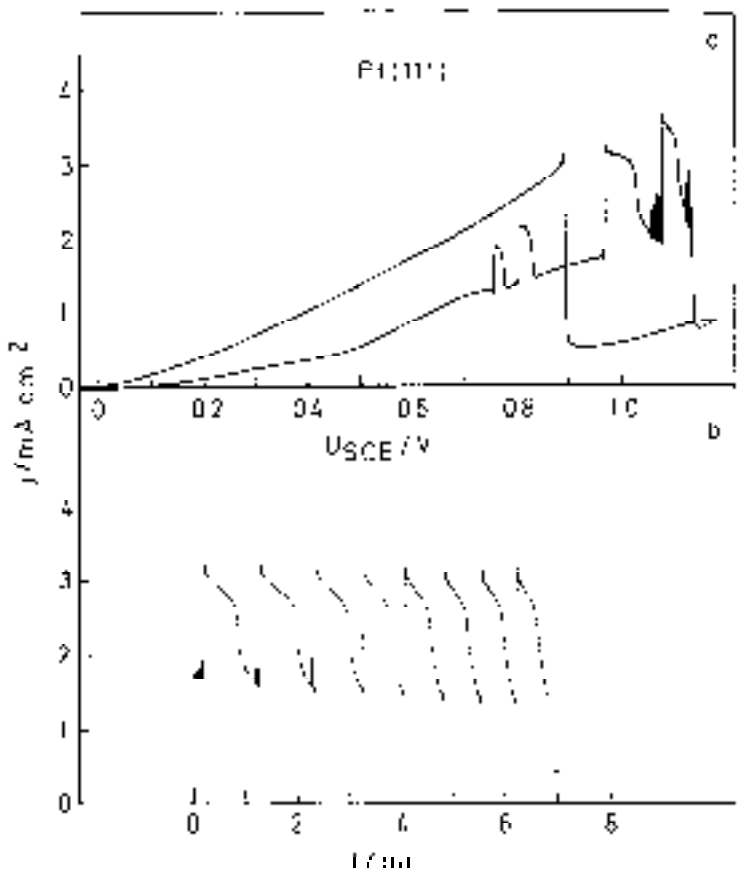


Figure 4-10: a) CV of FA oxidation on Pt(111) with external resistance $R_{ex} = 430\Omega$ at low FA concentration. Bulk solution: 0.05 M HCOOH, $10^{-3}$ M $HClO_4$. Scan rate 5 mV/s. Broad current oscillations appear on the anodic scan only.

ferent fixed potentials $U$ confirmed the conjecture: Fig. 4-12 evidences for the first time potentiostatic mixed-mode oscillations (MMOs) during the oxidation of formic acid.

For $U$ below 1 V, the MMOs consist of a large current spike followed by a number of small-amplitude peaks (there are at least 14 small peaks at $U = 0.913V$). As $U$ is further increased, the number of small spikes decreases until at $U = 1.2V$ the system exhibits period-1 oscillations. At no parameter value of $U$ the dynamics resembled that close to a homoclinic orbit. In addition, no quasiperiodic regimes between two mixed-mode states could be identified. Instead, aperiodic mixed-mode regimes were found to exist in very narrow potential regions between two successive mixed-mode states.

**Pt(110)**. At high concentration of HCOOH, both the $I - U$ characterstics and

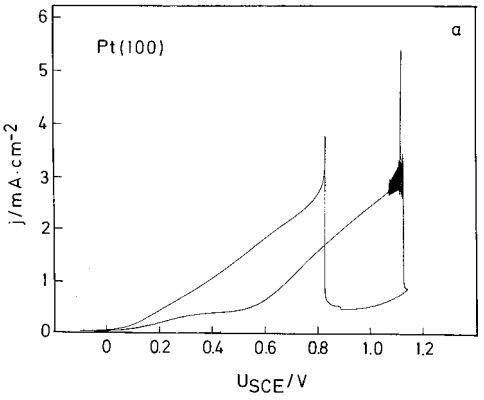


Figure 4-11: CV of FA oxidation on Pt(100) with external resistance $R_{ex} = 390\,\Omega$ at high FA concentration. Bulk solution: 1 M HCOONa, 0.5 M $H_2SO_4$. Scan rate 5 mV/s. Small and large current spikes appear on the anodic scan only.

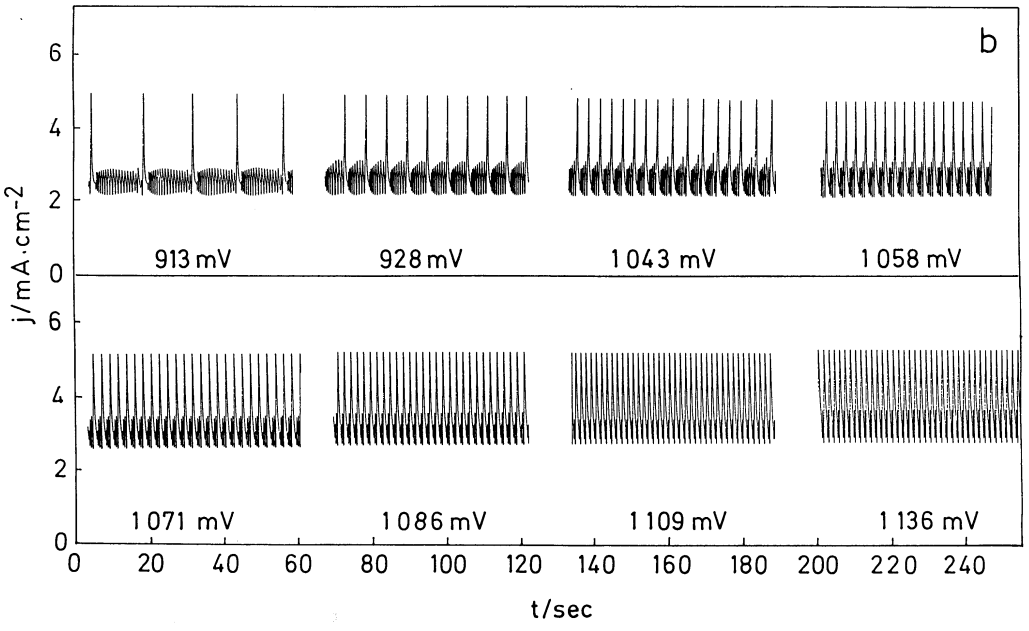


Figure 4-12: Mixed-mode oscillations at different constant potentials $U$.

the shape of the transient current oscillations on the (110) surface were found to be very similar to what is shown in Fig. 4-9. Therefore, these results are not reported in detail.

**Pt(111)**. Fig. 4-13a displays the high-concentration CV obtained with 220 Ω on the (111) surface. The anodic potential sweep reveals regular large-amplitude current spikes on peak II. As with the low HCOOH concentration, no current spikes were observed in the reversed potential scan (except for very small scan rates). For $U = 0.870V$, regular current oscillations were observed (Fig. 4-13b) which considerably decreased in period length during the stationary measurement. As for their waveform, the oscillations are relaxation-type oscillations; as seen on Pt(100), this type of oscillation is characterized by the presence of different time scales on which the underlying chemical processes evolve. The extremely rapid increase in current density is followed by an initially slow poisoning process which gets considerably accelerated for decreasing current densities. As found in Fig. 4-10b, the oscillation period on Pt(111) was found to be much larger than for the other two surfaces. When the scan was stopped immediately past the reactivation of the surface while scanning cathodically, stable oscillations were found after a comparatively long transient. This shows that - similar to Pt(100) - oscillatory behavior is present on both scans, but is suppressed due to kinetic reasons.

### 4.4.4 Bifurcation behavior

In dynamical systems theory, parameter regions of a distinct dynamics are conveniently shown in bifurcation diagrams. Varying a constraint a bifurcation is said to occur if the behavior of a dynamical system changes qualitatively. Fig. 4-14 shows such an experimental bifurcation diagram of the dynamics of the Pt(100) surface for a very low scan rate of the potential (5mV/s). It should be noted that due to the finite potential sweep rate Fig. 4-14 does not constitute a stationary bifurcation diagram as usually used in Nonlinear Dynamics. On the axes, the two major constraints, the normalized external resistance $R_{ex} \cdot A$ (just denoted as $RA$ in the figure) and the applied outer potential $U$, are plotted. The normalized resistance $RA$ was chosen to be independent of individual electrode geometries. In Fig. 4-14, for a given value of $RA$, the minimal and maximal potential $U$ at which current spikes were observed in the CV are indicated as solid lines regardless if observed during the anodic or cathodic scan. Thus, for fixed parameter values of $U$ and $RA$ between the two solid lines, current oscillations can be observed. The dotted line indicates the rapid increase in current in the cathodic scan, corresponding to the regeneration of vacant surface sites by desorption of OH. Since the bifurcation diagram was recorded at low HCOOH concentrations, even without external resistance current oscillations occur.

### 4.4.5 Stirring effects on oscillations

In the following, the influence of stirring on current oscillations is to be investigated. Fig. 4-15a displays the observed effect of stirring on period 1 oscillation on the (100) surface at low HCOOH concentration. When stirring is turned on, the current oscillations remain stable, but change their shape. When stirring is stopped again, the

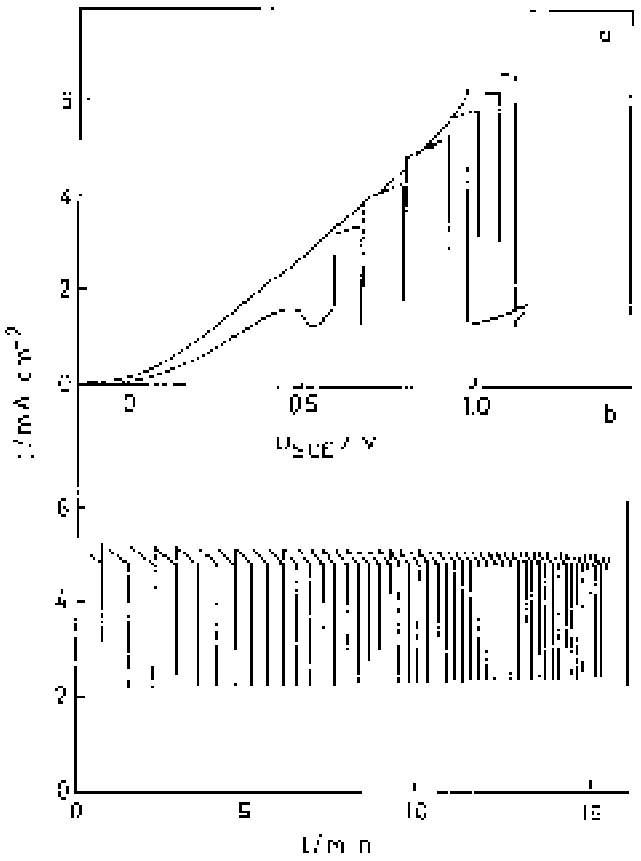


Figure 4-13: a) CV of FA oxidation on Pt(111) with external resistance $R_{ex} = 220\Omega$ at high FA concentration. Bulk solution: 1 M HCOONa, 0.5 M $H_2SO_4$ . Scan rate 5 mV/s. Broad current oscillations appear on the anodic scan only.

current oscillations relax back to a shape similar to the initial one. In Fig. 4-15b, current oscillations on the (111) surface were subjected to stirring. As can be seen, stirring results in an initial phase delay of the oscillation period. Similar to Pt(100), the oscillations remain stable without considerable change of their waveform.

In Fig. 4-16 the effect of stirring on stable mixed-mode oscillations was investigated on the Pt(100) surface. Mixed-mode oscillations (see Fig. 11b) are subjected to stirring after 42 sec (vertical line in Fig. 4-16). First, the mixed-mode character of the current oscillations vanishes by the disappearance of the small-amplitude peaks. Thereafter, the period 1 oscillations change their shape; the poisoning process becomes considerably delayed. About 80 sec after starting the stirring, the distorted period 1 oscillations are suppressed completely for about 400 sec. Finally, period 1 oscillations return which resemble those observed at low HCOOH concentration under stirring. The final period 1 oscillations are of larger period compared to the

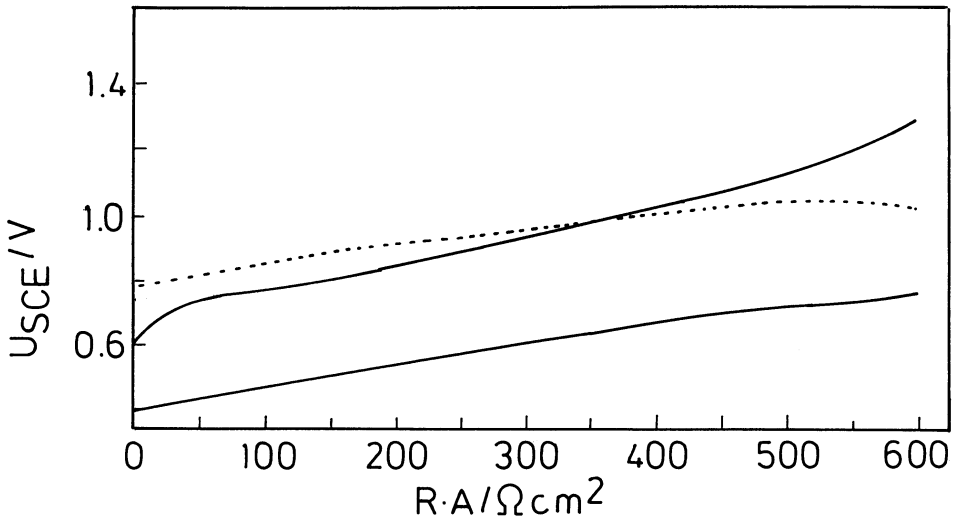


Figure 4-14: Experimentally measured bifurcation diagram for Pt(100) in 0.05 M HCOOH, $10^{-3}$ M $HClO_4$. The lower and upper solid line denote the low-potential and high-potential transition points between stable current behavior and sustained current oscillations, respectively, as found when scanning with 5 mV/s. The dashed line displayes the locations where the abrupt transition from low to high values of the current occurs when scanning cathodically.

inital mixed-mode oscillations. In order to rule out a simple parameter shift of the region of mixed-mode oscillations we investigated the system dynamics under stirred conditions for a variety of potentials $U$ and of HCOOH concentrations. Mixed-mode oscillations, however, were never found with stirred electrolyte.

## 4.5 Discussion and mechanistic considerations

### 4.5.1 Role of the ohmic resistance $R$

In the previous section, a systematic investigation of dynamical instabilities occuring during formic acid oxidation on the three single crystal surfaces Pt(100), Pt(110) and Pt(111) was reported. First the strong relation between electrochemical instabilities and the overall ohmic resistance $R$ was emphasized where the latter was given by the sum of the ohmic resistance of the bulk solution and an externally applied resistance $R_{ex}$. Unfortunately, the important role of the ohmic resistance $R$ and, accordingly, the role of the ionic concentration of the bulk solution were sometimes neglected in previous potentiostatic studies [112, 130, 131, 88, 114]. Fig. 4-7a and 4-7b clearly show that it is the ohmic resistance $R$ which accounts for the occurrence of electrochemical instabilities manifesting themselves in the case of formic acid not only by bistability, but due to appropriate slow chemical processes as sharp periodic current

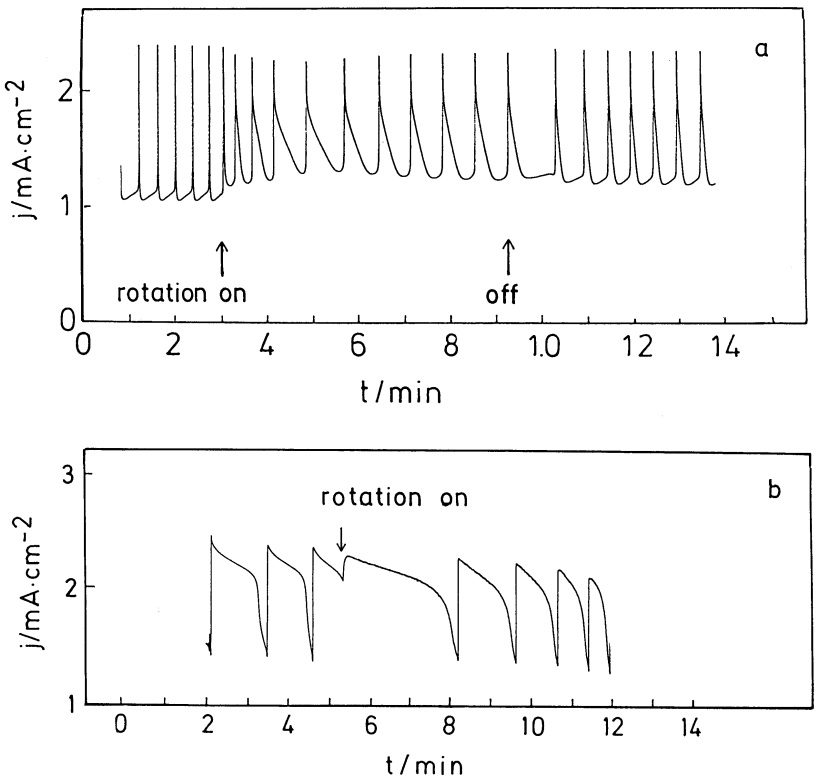


Figure 4-15: Stirring effects on sustained period-1 oscillations a) on Pt(100) in 0.05 M HCOOH, $10^{-3}$ M $HClO_4$, with $R_{ex} = 600\Omega$ at $U = 817mV$, b) on Pt(111) in 0.05 M HCOOH, $10^{-3}$ M $HClO_4$, with $R_{ex} = 700\Omega$ at $U = 1070mV$. The period-1 oscillations survive when the stirring is switched on.

spikes (Fig. 4-6,4-7a and 4-7b). The study further revealed that by application of an external ohmic resistance new, additional dynamic regimes are observable in the system. Moreover, we found that an external series resistor contributed considerably to the stability and reproducability of the observed dynamics. This is seen by the well reproducible current oscillations on Pt(110) and Pt(111) as well as the potentiostatic mixed-mode regimes on Pt(100).

### 4.5.2 The CO-oxidation system

The electrochemical oxidation of CO can be considered as a simplified subsystem of the formic acid oxidation system involving similar surface oxidation reactions of the surface poison, but differing in the source of the poison. Therefore, the investigation of the CO oxidation can provide valuable information on the reactivity of CO with oxygen containing species on the three Pt-single crystals.

Although the scanned CVs (Fig. 4-1) suggest the presence of a bistability in the

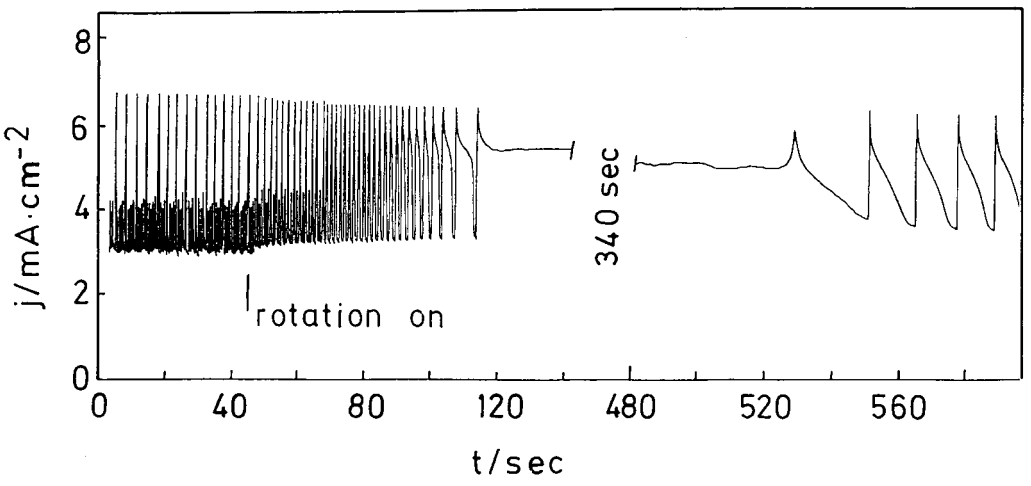


Figure 4-16: Stirring effect on mixed-mode oscillations on Pt(100) in 1 M HCOONa, 0.5 M $H_2SO_4$ with $R_{ex} = 280\Omega$ at $U = 984mV$. The mixed-mode oscillations are seen to be first quenched by stirring; after a transient, period-1 oscillations evolve.

system, the quasistationary (Fig. 4-1) and galvanostatic measurements indicate that the hysteresis is merely due to a slow CO adsorption process. If at all, true bistability only occurs in the absence of stirring.

An important conclusion from the foregoing discussion is that the CO oxidation system appears to be monostable for each single crystal. Consequently, a truly potentiostatic, i.e. purely chemical, instability - although feasible - seems not to be present. This result rules out certain suggestions as to the source of the instability of the formic acid system which have been put forward by different authors [112, 157, 158, 159, 160].

From the relative position of the CO removal peaks of the three surfaces, we further conclude that the CO poisoning of the surface becomes less pronounced in the order Pt(100), Pt(110) to Pt(111). A very dense monolayer of CO on Pt(100) obviously offers few bare sites for oxygen species to adsorb in contrast to Pt(111) where oxidation starts at smaller $U$.

The finite oxidation current at high values of $U$ indicates that the surface predominantly covered with OH allows for CO to be adsorbed and oxidized (asymmetric inhibition [161]).

### 4.5.3 A simple mechanism for the formic acid system

Most studies agree on the fact that formic acid oxidation proceeds via a dual path mechanism first proposed by Capon and Parsons [122, 152]. According to these authors, the initial adsorption of formic acid is followed by the formation of a reactive intermediate (presumably ·COOH) which is immediately oxidized further to $CO_2$, the final product. The reaction steps can be formulated as

$$HCOOH_{(aq)} \rightleftharpoons HCOOH_{ad} \tag{4.1}$$
$$HCOOH_{ad} \longrightarrow COOH_{ad} + H^+ + e^- \tag{4.2}$$
$$COOH_{ad} \longrightarrow CO_2 + H^+ + e^- \tag{4.3}$$

thereby assuming the oxidation of hydrogen radicals to be very fast. The rate of reaction 4.2 is certainly lower than that of reaction 4.3 since radical species are involved, but may be of comparable size to the adsorption reaction 4.1 depending on the diffusion thickness, the concentration of HCOOH and the number of available free surface sites. The reaction path given by reactions 4.2 and 4.3 is usually referred to as the direct path of formic acid oxidation. It is important to note that it is this reaction path which provides the necessary current density to account for the measured current peaks.

The dual path mechanism [122, 152] furthermore postulates a parallel reaction path to $CO_2$ via an intermediate which blocks the surface and impedes further adsorption of HCOOH. The nature of this poisoning species has long been the subject of intensive speculations [137, 162, 138, 163, 164]. Recent in-situ IR spectrometry, however, gave rise to believe that the dominating poisoning species is CO [20, 137, 116]. In the present study, we follow the most recent results and assume $CO_{ad}$ to be the only poison involved [131]. The poisoning reaction is assumed to follow the simple scheme

$$HCOOH_{ad} \longrightarrow CO_{ad} + H_2O. \tag{4.4}$$

At higher potential, $CO_{ad}$ is assumed to be removed through a surface reaction with adsorbed OH stemming from the oxidation of water molecules:

$$H_2O \rightleftharpoons OH_{ad} + H^+ + e^- \tag{4.5}$$
$$OH_{ad} + CO_{ad} \longrightarrow CO_2 + H^+ + e^- \tag{4.6}$$

Reactions 4.4, 4.5 and 4.6 are usually referred to as the indirect path of formic acid oxidation. Several authors [112, 157, 158, 159, 160] assumed the kinetics of reaction 4.6 to involve an additional free surface site in order to account for an autocatalytic feedback which in turn may cause a kinetic instability. In view of our results of the previous paragraph, however, we consider any additional kinetic assumption as irrelevant to the origin of oscillatory instabilities in the formic acid system. Again, we follow a simple mechanism and at this point neglect any further oxygen species such as $PtO, PtO_2$ or $PtO(O)$ [122, 165, 166] and subsurface hydroxide and oxygen [167] which were postulated to occur at double layer potentials $\phi_{dl} > 1.0V$. This simplification for the interpretation of oscillations can be justified as follows: Correcting the observed current oscillations by the $IR$ drop as given in section 3 one obtains the 'real' potential oscillations across the double layer $\phi_{dl}$. One finds that all current oscillations at fixed $U$ observed in this study correspond to oscillations of $\phi_{dl}$ in the

range of 0.1-0.7 V.

The findings in the preceding sections indicates that a region of NDR is required for instability in the FA system. Using the chemical reactions given above the occurrence of the NDR can now be made plausible. Whereas the direct oxidation path (reactions 4.1,4.2,4.3) shows a global positive potential characteristic, i.e. an increasing reaction rate as the applied potential is increased (positive slope of the $I/U$ curve), the combination of the direct path and reaction 4.5 leads to an N-shaped $I-U$ curve showing a region of NDR (negative slope). This is due to the OH poisoning of the surface which decreases the number of free sites available for the direct oxidation path.

With the chemical (pseudo)reactions given above a plausible simple model is obtained which should in principle be able to qualitatively account for the occurrence of oscillatory instabilities. We now turn to a more detailed discussion of the current peaks observed in the CV and try to come up with a plausible interpretation in terms of the chemical reaction steps of the simple model.

### 4.5.4 Peak I and II

For $-0.1$ V$< U <$ 0.5 V, i.e. the potential range of peak I, the residual number of free surface sites determines the rate of the direct oxidation path and simultaneously the measured current density on all three surfaces. For values of $U >$ 0.5 V, OH is adsorbed on the surface (reaction 4.5) regenerating an increasing number of free surface sites via reaction 4.6. Thus, the rate of the direct path increases considerably. As $U$ increases further, all poisoning CO is removed, and the surface becomes blocked by the OH species. This scenario is believed to equally hold for all three surfaces during the anodic scan. Fig. 4-3, however, shows pronounced discrepancies between the surfaces during cathodic sweeping which can be made plausible as follows: Pt(111) exhibits a lower affinity towards CO thus showing incomplete poisoning by CO [168, 169, 132] (see also the results on CO oxidation). In contrast, Pt(100) was found to be completely blocked by the poisoning species [168, 169, 132]. Furthermore, the direct path was also found to proceed faster on Pt(100) than on Pt(111) [169]. This structural difference leads to a vanishing peak I, but to a pronounced peak II for Pt(100) . The reverse, however, holds true for Pt(111). Pt(110) appears to behave similar to Pt(100). It should be noted that the CV of Pt(111) in Fig. 4-3 differs from those measured in previous studies [132, 135] in that the current density of peak IV/V in the cathodic scan was found to be much larger than that of peak I in the anodic scan.

### 4.5.5 Peak IV and V

In section 4, we have shown the splitting of the large current peak on the cathodic scan of Pt(100) and Pt(110) into peak IV and V and mentioned results on the dependence of these peaks on the scan rate and anodic reverse potential. By means of our simple model mechanism, we interpret the rapid current increase during the cathodic scan as the very rapid regeneration of a large number of free surface sites resulting in a high rate of the direct oxidation path. As $U$ decreases, the surface becomes more and more

poisoned by CO via reaction 4.4 until the current density vanishes. This qualitative interpretation is equally valid for all three surfaces and therefore does not account for the structural effects leading to the two distinct peaks IV and V. It is obviously necessary to reconsider possible additional reaction steps which are consistent with our experimental findings.

The dependence of peak IV on the upper limit potential shows a relationship between the amount of deposited oxygen species and peak IV. Compared to adsorption, the desorption of the oxygen species requires a smaller potential. Consequently, there is an overlap of the potential regions where the surface oxygen species are still present, yet where formic acid restarts to deposit on bare sites. From this, it is plausible to identify peak IV with the reaction of re-adsorbed HCOOH and reactive surface oxides which remained on the surface. We therefore consider an additional chemical reaction step such as

$$HCOOH_{ad} + Pt - OH \longrightarrow H_2O + CO_2 + Pt + H^+ + e^- \tag{4.7}$$

to be involved in the chemical processes occurring at peak IV. The experimental finding that peak IV increases with increasing scanrate is consistent with the assumption that at least a part of the charge transfer involves preadsorbed species. Peak V almost coincides with peak I in potential suggesting its origin to be the direct oxidation path as discussed for peak I (reactions 4.2,4.3).

It follows that Peak IV originates in the oxidation of FA in the presence of adsorbed oxygen species, whereas Peak V stems from the direct FA oxidation while at the same time the surface gets slowly poisoned by CO.

### 4.5.6 Oscillatory instabilities

We have shown oscillatory behavior of the current density on the three low-index Pt single crystals at both low and high HCOOH concentrations. In general, current oscillations at high HCOOH concentration proved to be more stable and better reproducible than at low concentrations.

On the basis of the experimental results, the occurence of the current oscillations can be described in physicochemical terms as follows: For an appropriate constant outer potential $U$ and a sufficiently large ohmic resistance $R$, the total current density $I$ based on the direct oxidation path decreases due to CO poisoning of the active surface. Thereby, the initially low double layer potential $\phi_{dl} = U - IR$ increases leading to the adsorption of OH. Due to $OH_{ad}$ even more sites are blocked, which in turn lowers the current, increases $\phi_{dl}$, enhances OH formation and leads to an overshooting of $\phi_{dl}$ on a fast time scale. Then, however, the reactive removal of CO (indirect path) sets in, regenerating vacant surface sites. This results in an increase of $I$ and, due to the electrical relation given above, in a decrease of $\phi_{dl}$ until all OH has desorbed and the slow CO poisoning process resumes.

In section 4, it was shown that the oscillatory potential range as well as the waveform of the current oscillations were very similar on both the cathodic and the anodic scan. This suggests the oscillations on either scan to be caused by the same

instability. However, why is it that oscillatory spikes are visible over a broad potential range on the cathodic scan, but hardly appear on the anodic scan? The reason for that must be sought in the different initial conditions that hold when the double layer potential enters the unstable potential range. On the anodic scan, the surface is almost completely blocked by CO. Therefore, the CO coverage is too high for sustained oscillations to occur. Scanning anodically, a slow removal of CO by adsorbed OH occurs on the cathodic flank of peak II. Still, the transient behavior of the current, i.e. the time until the coverages of CO and OH necessary for oscillations are reached, is long compared to the time the system needs to leave the oscillatory potential range at the chosen sweep rate. Thus, no current spikes are seen scanning in anodic direction. On the reversed scan, however, a large number of free surface sites is rapidly regenerated after the first OH desorption peak. Since on Pt(100) the rate of poisoning is high [168, 169, 132] , the time to reach the CO coverage necessary for oscillations is short compared to the time the system spends in the oscillatory potential region. Consequently, sharp current spikes are visible.

On Pt(111), the rate of poisoning (process 4.4) is comparatively slow [168, 169, 132] leading to the characteristic oscillatory waveform shown in Fig. 4-10b and Fig. 4-13b. The low affinity of Pt(111) towards CO can also be used to explain the absence of current spikes on the cathodic scan (see Fig. 4-10a and 4-13a). The reasoning is similar to the one discussed for Pt(100): As soon as the surface gets reactivated (at $U = 0.9$ V in Fig. 4-10a, at $U = 0.95$ V in Fig. 4-13a), the double layer potential is too low for oscillations to occur due to the high $IR$ drop. Now, the transient time until the CO coverage has reached the threshold value necessary for current oscillations is long compared to the time the systems spends in the oscillatory potential region. Further evidence in favor of this interpretation is provided by the experimental finding that current oscillations eventually evolve if the cathodic sweep is stopped after reactivation. Compared to Pt(100), current oscillations on Pt(111) are in general less stable and show transient behavior over a considerable potential range ending up on the OH-poisoned state. In general, the presence and absence of current spikes depends on the relative rate of scanning and induction of oscillations.

The findings on Pt(110) (Fig. 4-9a) best allow a conclusion on the type of bifurcations that lead to oscillatory instabilities. At the lower limit of the oscillatory potential region ($U = 0.68$ V), oscillations emerge with very small amplitude and high frequency suggesting a Hopf bifurcation as conjectured in the case of Pt(100). At the upper limit, however, the relaxation oscillations disappeared at finite amplitude and long period. From Nonlinear Dynamics it is well known that this is typical for a saddle-loop bifurcation. Similar to Pt(111) at low HCOOH concentration, the oscillations are transient and die on the low current branch.

At higher HCOOH concentrations, the (100) surface was found to exhibit a sequence of mixed-mode oscillations (MMOs) characterized by large current spikes followed by an increasing number of small high-frequency spikes for lower values of the applied potential $U$. This is - to our knowledge - the first observation of MMOs during formic acid oxidation under potentiostatic control. Previous work on formic acid dealing with MMOs focused mainly on galvanostatic conditions [159, 158, 160].

From the experimental findings it would be daring to settle the question of what

type of bifurcation scenario leads to the formation of mixed-mode oscillations. We can, however, certainly assume an additional negative feedback variable (chemical species) to be crucial to the dynamics, which together with the negative and the positive feedback involved in the period-1 oscillations gives rise to two interacting oscillators and consequently to mixed-mode oscillations.

### 4.5.7 Stirring effects

Regardless of the orientation of the single crystal surfaces, period-1 oscillations during formic acid oxidation were found to survive while stirring. This is in agreement with early work on polycrystalline Pd [112], but in contrast to recent results on Pt(100) [88] where stirring was found to suppress sustained oscillations. On Pt(100), the oscillatory waveform proved sensitive towards stirring in that it became less relaxational; the emerging oscillatory waveform resembled that which was found if , under unstirred conditions, one scanned to smaller potentials $U$. Thus, the set of chemical species essential to the oscillatory period-1 instability seems not to include any solution species as, at higher stirring rates, the solution species near the double layer become either quenched to their bulk concentration due to rapid mass transport or are rapidly removed from the surface.

From the global disappearance of mixed-mode oscillations on Pt(100) when subject to stirring, we can conclude that the set of chemical species essential for the occurrence of the small-amplitude spikes does involve at least one solution species. In view of the foregoing discussion on the origin of the MMOs we could identify this solution species as a candidate for an additional (negative-feedback) species essential for the dynamics of MMOs, but nonessential for period-1 oscillations. Under stirred conditions this solution species is not available as a dynamical variable so that only period-1 oscillations remain. The long transient before stable oscillations return is presumably the consequence of slowly reestablishing concentration conditions near the double layer necessary for oscillations.